Search for the Proton Decay in the large liquid Scintillator Detector LENA

A Feasibility Study

Diploma Thesis
by
Teresa Marrodán Undagoitia

Physik-Department E15
Technische Universität München
May 2005

Abstract

The LENA (**L**ow **E**nergy **N**eutrino **A**stronomy) detector is proposed to be a large-volume liquid-scintillator device which will be highly suitable for the investigation of a variety of topics in astrophysics, geophysics and particle physics. In a cylindrical tank of about 100 m length and 30 m diameter, $\sim$ 50 kt of PXE will act as scintillating material while 12 000 photomultipliers will readout the signals. To reduce background radiation, in particular atmospheric muons, possible locations for this detector are deep underground or deep sea laboratories. In this thesis, the potential of such a detector concerning the search for proton decay in the SUSY favored decay channel $p \rightarrow K^+\overline{\nu}$ is investigated. Based on Geant4, Monte Carlo simulations of the proton decay in the LENA detector as well as of the background radiation in the detection energy windows have been developed. For both proton decay and background studies, 20 000 events have been simulated, taking into account quenching, absorption and scattering effects within the liquid scintillator and the effects of the photomultipliers in the signal output. From these simulations an efficiency of 65% for the detection of a possible proton decay has been determined. Within ten years of measuring time a lower limit for the proton lifetime, concerning the decay channel investigated, of $\tau > 4 \cdot 10^{34}$ y could be reached.

Contents

List of Figures

Chapter 1

Introduction

With the observation of solar neutrinos, pioneered by R. Davis with the Homestake experiment [1] in the early 1970s and the observation of neutrinos emitted in a supernova in 1987 [2][3][4][5] a new window was opened for Astronomy.

In recent years important discoveries in the field of low energy neutrino physics have been achieved. The Sudbury Neutrino Observatory (SNO) [6] has provided a solution to a 30-year old mystery, the puzzle of the missing solar neutrinos [7][8][9]. The solution does not lie in the Sun, but in the neutrinos, which change its flavour as they travel from the core of the Sun to the Earth. Therefore, a clear transition from ν_e to $\nu_{\mu,\tau}$ has been demonstrated [10]. Nowadays, the pp-cycle has been recognized as the main energy source of the sun and the experimental uncertainty on the ^{8}B neutrino-flux is already below the theoretical one.

In the KamLAND experiment the disappearance of $\overline{\nu}_e$, emitted by nuclear power reactors at an average distances of $\sim$ 180 km, has been observed [11]. These observations can be interpreted as evidence for neutrino oscillations, which are a direct consequence of neutrino masses and neutrino mixing. In addition, there is evidence for neutrino oscillations from atmospheric neutrino measurements performed in Superkamiokande [12] and other experiments [13]. In this case the disappearance of ν_μ has been observed. Accelerator experiments can also search for neutrino oscillations. For example the LSND [14] experiment claims an evidence. The experiment MiniBooNE [15] at Fermilab will be performed to further verify this measurement.

The weak eigenstate neutrinos, which are produced with a definite lepton flavour in weak transitions, are mixtures of the neutrinos of definite masses.

This mixing can be represented by the matrix [16][17]:

$$\begin{pmatrix} \nu_e \\ \nu_\mu \\ \nu_\tau \end{pmatrix} = \begin{pmatrix} U_{e1} & U_{e2} & U_{e3} \\ U_{\mu 1} & U_{\mu 2} & U_{\mu 3} \\ U_{\tau 1} & U_{\tau 2} & U_{\tau 3} \end{pmatrix} \cdot \begin{pmatrix} \nu_1 \\ \nu_2 \\ \nu_3 \end{pmatrix}$$

or parametrized in the form:

$$\begin{pmatrix} \nu_e \\ \nu_\mu \\ \nu_\tau \end{pmatrix} = \begin{pmatrix} 1 & 0 & 0 \\ 0 & c_{23} & s_{23} \\ 0 & -s_{23} & c_{23} \end{pmatrix} \begin{pmatrix} c_{13} & 0 & s_{13}e^{-i\delta} \\ 0 & 1 & 0 \\ -s_{13}e^{i\delta} & 0 & c_{13} \end{pmatrix} \begin{pmatrix} c_{12} & s_{12} & 0 \\ -s_{12} & c_{12} & 0 \\ 0 & 0 & 1 \end{pmatrix} \begin{pmatrix} \nu_1 \\ \nu_2 \\ \nu_3 \end{pmatrix}$$

where $s_{ij} = \sin\Theta_{ij}$ and $c_{ij} = \cos\Theta_{ij}$ with rotation mixing angles Θ_{ij}. The imaginary phase δ can describe a possible CP-violation. The general form of this mixing matrix includes two additional phases, called Majorana phases.

From solar, reactor and atmospheric neutrino measurements the mass squared differences and the mixing angle between the first and the second family, as well as between the second and the third family have been determined. However, the coupling parameter between the first and the third family is still unknown and the absolute values of neutrino masses are also not precisely determined, as oscillation experiments measure only mass squared differences. An upper limit for the sum of neutrino masses of about 2.2 eV have been achieved in different Tritium experiments [18][19] and also cosmological experiments have given limits of $m_\nu \sim 1$ eV, being modell dependent [20]. In addition, the term with the mass difference $\sqrt{\Delta {m_{atm}}^2}$ allows to set a lower bound on the absolute neutrino mass. At least one of the neutrino mass eigenvalues should satisfy an inferior mass $m_\nu > 50$ meV. Future neutrino experiments aim to measure the mentioned missing neutrino properties: the mixing angle Θ_{13} and absolute neutrino masses.

Neutrinos can now be used as probes in order to receive information from astrophysical objects, which otherwise would be unaccessible. Thus, new research fields have been opened, e.g., supernovae neutrinos, geoneutrinos or the search for proton decay. In order to have high statistics in those measurements, a new generation of large neutrino telescopes is required. In this line, large ($\sim$Mt) water or ice Cherenkov detector or a ($\sim$100 kt) liquid argon Time Projection Chamber (TPC) are going to be investigated.

With the experience accumulated with liquid scintillator detectors, for example BOREXINO [21] at the Italian Gran Sasso underground laboratory, the optical properties of a liquid scintillator based on PXE are basically understood. The electronics required is already developed and the volume required to compete with a Mt water Cherenkov detector would be smaller ($\sim$50 kt). That motivates detailed feasibility studies of the potential of such a liquid scintillator detector.

A large liquid scintillator detector is an interesting instrument, especially to look for several branches of possible proton decay events, which are difficult to observe in water Cherenkov detectors. In the present work, first a summary of the proposed LENA (**L**ow **E**nergy **N**eutrino **A**stronomy) detector physics program is given. Thereafter, a description of the detector and its possible location are presented. Then, a phenomenological theoretical framework of the proton decay into the channel $p \to K^+\overline{\nu}$ is explained. The main part of the thesis will be a detailed description of the simulation of the possible proton decay and the analysis of the first simulation data obtained including a discussion about background suppression. The analysis of this data will result in a derivation of the efficiency of the LENA detector and its sensitivity for the proton decay.

Chapter 2

The LENA Experiment

LENA (**L**ow **E**nergy **N**eutrino **A**stronomy) is a large-volume liquid-scintillator neutrino telescope planned to be built in the near future. First of all, this chapter reviews the physics program of the LENA project and then explains the design of the detector and the possible locations under consideration.

2.1 Physics

The physics program of LENA covers a great variety of topics which can be devided into three fields: astroparticle physics, geophysics and particle physics. This section briefly describes some of the main subjects of these three fields, giving the current status of other existing experiments on measuring these processes and showing the potential of the LENA detector.

2.1.1 Supernovae Relic Neutrinos

It is generally believed that core-collapse supernovae have ocurred throughout the Universe since the formation of stars. In such an explosion a great quantity of energy is released, most of it, 99% of its binding energy, in the form of neutrinos. Neutrinos from a supernovae explosion were measured once, in the case of the supernova SN1987A [2][3][4][5]. There should exist a diffuse background of supernova relic neutrinos (SRN) and its detection would deliver valuable information about the history of star formation in the Universe.

The measurement of the SRN flux is one of the aims of LENA. All types of neutrinos and antineutrinos are emitted in a core-collapse supernova but $\overline{\nu}_e$ is the most likely to be detected. The currently best value for the $\overline{\nu}_e$ flux comes from the Superkamiokande detector and gives an upper limit of 1.2 $\mathrm{cm}^{-2}\mathrm{s}^{-1}$

with a threshold of 19.3 MeV [22]. With LENA the sensitivity for the SRN search would be drastically improved, as the delayed coincidence between the prompt positron and the captured neutron in the inverse beta decay reaction, $\overline{\nu}_e + p \rightarrow n + e^+$, can be utilized. These two delayed signals would strongly reduce the background and an energy threshold of ~ 9 MeV should be achieved. No lower threshold is reachable because of the ubiquitous $\overline{\nu}_e$ from nuclear plants. According to the most recent models [23], the predicted SRN flux at 10 MeV is about 0.6 $\mathrm{cm^{-2}s^{-1}MeV^{-1}}$ and LENA should observe an event rate of about 4/year.

2.1.2 Supernovae Neutrinos

What happens in a supernova core? [24][25][26] Core-collapse supernovae are the final stage of a star which has a mass above about eight solar masses. When its nuclear fuel is consumed and it is no longer supported by the release of nuclear energy, its core collapses and releases a huge amount of energy, most of it in the form of neutrinos. This causes a blast wave that ejects the star's envelope into interstellar space. The result of the collapse may be, in some cases, a rapidly rotating neutron star that can be observed many years later as a radio pulsar or even a black hole.

In case of a supernova explosion at the center of our galaxy, i.e., at a distance of ~ 10 kpc, a neutrino burst of ~ 15000 events can be expected in the LENA detector. Using an organic scintillator containing ^{12}C allows the distinct flavour-specific neutrino and antineutrino detection by the following reactions:

$\overline{\nu}_e + p \rightarrow n + e^+$ (Q=1.8 MeV)
$\overline{\nu}_e + {}^{12}\mathrm{C} \rightarrow e^+ + {}^{12}\mathrm{B}$ (Q=17.3 MeV)
$\nu_e + {}^{12}\mathrm{C} \rightarrow e^- + {}^{12}\mathrm{N}$ (Q=13.4 MeV)
$\nu_x + {}^{12}\mathrm{C} \rightarrow {}^{12}\mathrm{C}^* + \nu_x$ with ${}^{12}\mathrm{C}^* \rightarrow {}^{12}\mathrm{C} + \gamma$
$\nu_x + p \rightarrow \nu_x + p$ (elastic scattering)
$\nu_x + e^- \rightarrow \nu_x + e^-$ (elastic scattering).

The dominant contribution comes from the first reaction because the inverse beta decay for $\overline{\nu}_e$ has the largest cross-section. Using the delayed coincidence between the prompt positron and the neutron capture on hydrogen, the $\overline{\nu}_e$ contribution can be distinguish from the others. The next two reactions can be tagged by the re-decay of the daugther nuclei, ^{12}B (β^-, $\mathrm{T_{1/2}} = 20$ ms) and ^{12}N (β^+, $\mathrm{T_{1/2}} = 11$ ms). As all the neutrino flavours participate in the fourth reaction, information on the total SN neutrino flux

is received. In the last two reactions the recoil energy of protons or electrons can be detected and give the neutrino spectrum for all flavours.

Observation of such a ν burst would reveal important details of the explosion mechanism. In addition, the $\overline{\nu}_e$ energy spectrum would show wiggles which are caused by oscillation matter effects when neutrinos cross the Earth before entering the detector depending on the ν-mass hierarchy and on the value of Θ_{13} [27][28]. From such a measurement ν-oscillation parameters and information about the mass hierarchy can be derived.

2.1.3 Solar Neutrinos

The precise knowledge of the functioning of the solar energy release is a crucial question in astrophysics. The future solar neutrino experiments, BOREXINO and KamLAND are supposed to measure directly the solar ^{7}Be-ν flux for the first time. However, the pep- and CNO-fluxes are faint and the always present cosmic ray background make those measurements very difficult [29]. With LENA in a fiducial volume for solar neutrinos of about $18 \cdot 10^3$ m^3, the solar ν rates would be $\sim$ 5400 d^{-1} for ^{7}Be-ν, 150 d^{-1} for pep-ν and 210 d^{-1}for CNO-ν. After measuring these fluxes and together with the known solar luminosity and ν-oscillation parameters, the fundamental pp-flux can be determined wih an accuracy of better than 0.5%.

Due to the high statistics measurement of the ^{7}Be-ν flux, a test on temporal fluctuations of the solar density profile can be achieved with high precision. Such temporal density fluctuations could eventually be created by solar g-mode waves, which are not observed so far by helioseismology. A further observation could be a day-nigth asymmetry on the ^{7}Be flux (1%) due to the MSW effect [31][32] in the earth [30]. In addition, the predicted solar MSW effect for low energy ($E_\nu < 6$ MeV) in ^{8}B can be searched for. Also transitions $\nu_{eL} \rightarrow \overline{\nu}_{eR}$ which entail helicity-flipping $\Delta L_e = 2$ can be investigated [33].

2.1.4 Geoneutrinos

The sources of the thermal heat flow emitted by the Earth (60 mW/m^2 or 40 TW, integrated for the hole surface [34]) are not completely understood. One partial explanation is the heat produced in the decay of natural radiactive isotopes. In order to quantitatively know this radiogenic contribution a measurement is necessary. In the Uranium and Thorium chains, neutrinos are emitted in beta decays. These so-called geoneutrinos have energies up to

3.2 MeV and could be detected by the inverse beta decay $\overline{\nu}_e + p \rightarrow n + e^+$. This reaction has however an energy threshold of 1.8 MeV. One can distinguish them from reactor neutrinos which have energies up to about 8 MeV but it depends on the detector location and the statistics.

With a large detector like LENA the flux of geoneutrinos coming from the crust, the mantle and the core of the Earth can be measured and the abundances of Uranium, Thorium and Potassium can be derived. An event rate of $\sim$ 3000 y^{-1} is estimated. For LENA an angular distribution of 26° (half cone aperture). Details can be found in the thesis of Kathrin Hochmuth [35].

2.1.5 Long Baseline Experiments

In case a high energy neutrino beam is directed to LENA, the detector could also be used for the long baseline oscillation studies [36] including the matter effects and eventually for the search for CP-violation in the leptonic sector. Muon events should be separable from electron events due to their different lenghts in the detector and by observing the succeding decay of the muon. For this purpose the axis of the detector should be placed parallel to the neutrino beam.

2.1.6 Atmospheric Neutrinos

With LENA, the low energy part of the spectrum of atmospheric neutrinos could be explored in more detail. The quasi-elastic reactions $\overline{\nu}_e + p \rightarrow n + e^+$ and $\overline{\nu}_\mu + p \rightarrow n + \mu^+$ could be used to measure the corresponding antineutrino fluxes in the energy region between $\sim$ 100 MeV and 1 GeV. For the second reaction, as the μ^+ decays after 2.2 μs the $\overline{\nu}_\mu$ would be tagged by a three fold delayed coincidence. Thus, one can separate those events clearly from $\overline{\nu}_e$ events.

At 200 MeV, the oscillation lenght of $\overline{\nu}_e$ due to $\Delta {m_{12}}^2$ should be around 7000 km and this should lead to oscillations of the type $\overline{\nu}_e \leftrightarrow \overline{\nu}_{\mu,\tau}$. At 1 GeV however, the oscillation lenght is about at 35000 km and the oscillation probability should become significantly smaller. On the other hand $\overline{\nu}_\mu$ oscillation into $\overline{\nu}_\tau$ due to the $\Delta {m_{23}}^2$ splitting should always be present and lead to a depletion of the $\overline{\nu}_\mu$ flux. This implies, that a well defined energy dependent ratio $\overline{\nu}_e/\overline{\nu}_\mu$ due to the various oscillations should be observable in LENA.

2.1.7 Proton Decay

In the context of Grand Unified Theories, the proton is predicted to decay leading to a non-conservation of the baryon number. The simulation of the proton decay in LENA constitutes the body of this thesis. The theoretical frame where predictions of proton decay appear will be presented as well as the details of the simulation and first results.

2.2 LENA Detector

2.2.1 Detector Design

The LENA detector is planned [37] to have a cylindrical shape with an outer volume of $\sim$ 100 m length and 30 m diameter. In the figure 2.1 an artistic representation of the LENA detector is given.

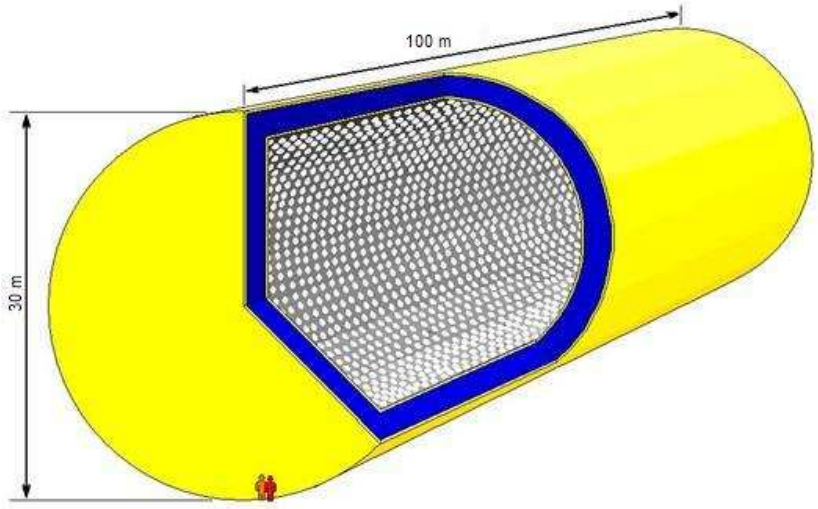

Figure 2.1: Artistic representation of the LENA detector.

This large volume will be divided into two parts, an inside one of about 13 m radius that will contain approximately 50 kt of liquid scintillator while the outside part (13 – 15 m radius) will be filled with water. Using the Cherenkov effect, the water will act as muon veto. A fiducial volume for proton decay will be defined having a radius of 12 m. This radius will be determined offline by using the time of flight and the pulse height information of each photomultiplier. Covering about 30% of the surface, 12 000 photomultipliers of 50 cm diameter each will collect the light produced by

the scintillator. To have an idea of this structure in figure 2.2 a section of the outer part is ilustrated.

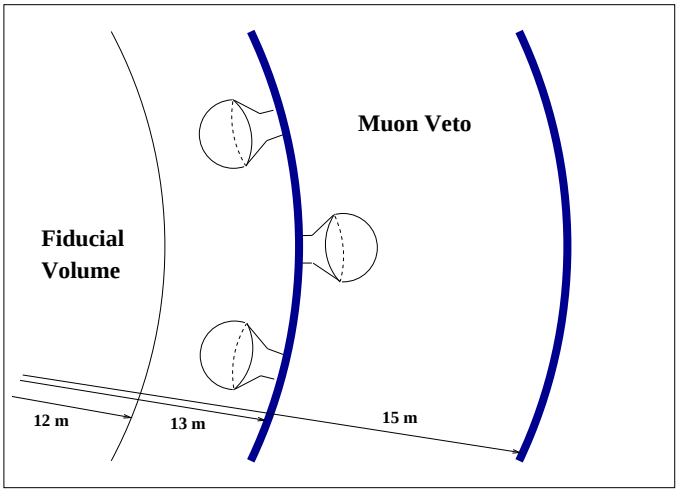

Figure 2.2: Lena detector section. The fiducial volume shown corresponds to the proton decay research and will be defined in the data analysis by using the time of flight and pulse high information.

2.2.2 A liquid Scintillator based on PXE

PXE (phenyl-o-xylylethane, $C_{16}H_{18}$) is foreseen as scintillator solvent because of its high light yield and its save handling procedures. Figure 2.3 shows the molecular structure of PXE.

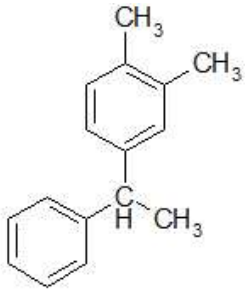

Figure 2.3: PXE Formula.

The optical properties of a liquid scintillator based on PXE have been investigated in the Counting Test Facility (CTF) for BOREXINO at the Gran

Sasso underground laboratory [38]. A yield of 372 ± 8 photoelectrons per MeV (pe/MeV) has been measured in this experiment with an optical coverage of 20%. The attenuation length of ∼ 3 m (at 430 nm) was substantially increased to ∼ 12 m purging the liquid in a weak acidic alumina column [38]. With these values an expected photoelectron yield of ∼ 120 pe/MeV can be estimated for events in the center of the LENA detector. Currently the optical properties of mixtures of PXE and derivatives of mineral oils are under investigation [39].

2.3 Possible Locations of the Detector

Two possible locations for this detector are currently under discussion. The first site considered is an underground mine in the center of Finland (Pyhäsalmi, CUPP[1]). The map of the location is given in figure 2.4.

Figure 2.4: Map of the Pyhäsalmi mine in Finland.

[1]Center of Underground Physics in Pyhäsalmi.

The mine is in a depth of 1450 m which corresponds to a shielding of cosmic rays of $\sim$ 4000 m.w.e.. The muon flux has been measured at the greatest depth and is less than 10^{-4} $m^{-2}s^{-1}$. Because of being far away from nuclear power plants, the reactor $\overline{\nu}_e$ background is low. The accessibility to the mine is via a truck road and a lift that covers all the way down. The liquid scintillator could be transported via railway to the surface of the mine and then loaded into the experimental area by an already existing direct pipeline. The mine also has no fundamental problems concerning the excavation of new caverns in the size required by the LENA detector. The construction of LENA in Pyhäsalmi is feasible due to all the advantages mentioned.

The second site could be under water close to the coast at Pylos in Greece ("The NESTOR Independent Institute for: Deep Sea Research Technology and Neutrino Astroparticle Physics"). The NESTOR experiment takes advantage of the unique fact that it is deployed near the deepest part in Europe (depth up to 5200 m). At a distance of about 14 km off the shore, at a water depth of 4000 m there is a fairly large abyssal plane that is perfectly suited for several deep-sea installations. Also this site is favored because of being away from nuclear power plants.

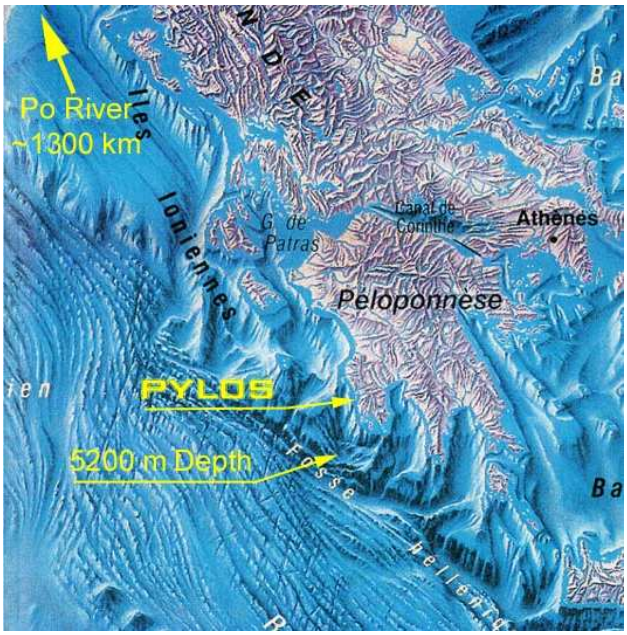

Figure 2.5: Map of the coast of Greece.

Chapter 3

Theoretical Predictions of Proton Decay

After the unification of the electromagnetic with the weak force by Glashow, Weinberg and Salam [41][42][43] between 1961 and 1969, the next goal was the unification with the strong force within the Grand Unified Theories (GUTs). One of the earliest of such theories placed the $SU(3)_c \otimes SU(2)_L \otimes U(1)_Y$ Standard Model groups into a single SU(5) [44][45]. For this model, the quarks and the leptons can be accomodated in the $\overline{5}$- and 10-representations. However, other unification symmetry groups, like SO(10) where one family of quarks and of leptons sit in the 16-dimensional spinor representation, can be constructed and are currently studied [40].

A prominent feature of the GUTs is the non-conservation of the baryon (B) and lepton (L) numbers [44][45] which implies the possibility of nucleon decay. The particles into which the nucleon may decay are limited by symmetry principles, for example $\Delta(B - L) = 0$. In GUT SU(5) nucleons decay via the exchange of gauge bosons with GUT scale masses (M_G), resulting in dimension-6 baryon-violating operators suppressed by a factor $(1/M_G^2)$. The nucleon lifetime is calculable and given by $\tau_N \propto M_G^4/(\alpha_G^2 m_p^5)$ where α_G and m_p are the unification constant and the mass of the proton respectively. The dominant decay mode of the proton (or baryon-violating decay mode of the neutron) depends on the value of the grand unification mass ($M_G > 10^{14}$ GeV) and on α_G. If the masses of the new gauge fields which mediate baryon number violating processes were not very large, the proton would decay at an unacceptably fast rate.

A measurement of such a rare event as proton decay could be a test of the validity of those theories and further evidence of the existence of physics

beyond the Standard Model. Experimental searches for nucleon decay began with the Kolar Gold Mine, Homestake [46], Soudan [47], NUSEX [48], Frejus [49], HPW [50] and IMB [51] detectors. Until now, no proton decay event has been measured. Today, the most stringent limits are provided by Superkamiokande.

In this chapter, together with a description of the different GUT predictions for the proton decay, the current best experimental lower bounds for the proton lifetime are presented.

3.1 Grand Unified Theories

In the minimal GUT SU(5) [52], the nucleon decays via exchange of gauge bosons with GUT scale masses ($\sim 10^{15}$ GeV). For the proton, the dominant decay mode predicted is $p \to e^+\pi^0$ with a lifetime of $\tau \sim 10^{31}$ y.

The Super-Kamiokande Collaboration has set the current lower limit for this channel to $\tau > 5.4 \cdot 10^{33}$ y at 90% confidence level (C.L.) [53][54]. This result together with the fact that, in this theory, the three running coupling constants do not meet in a single point give reasons to look also at other theories.

3.2 Supersymmetry

In Supersymmetric GUTs (SUSY), the nucleon decay is affected by operators of dimensions 4, 5 and 6. They involve B- and L-violating processes but conserve B − L. The M_G is of the order of $3 \cdot 10^{16}$ GeV. For the proton decay mode $p \to e^+\pi^0$ a lifetime of $\tau \sim 5 \cdot 10^{35\pm1}$ y has been calculated. This rather long lifetime results from the large value of the unification mass, M_G, given by those theories. For the decay channel $p \to K^+\overline{\nu}$ ($\overline{\nu} = \sum_{\{i=e,\mu,\tau\}} \overline{\nu_i}$) a range for the lifetime $\tau \sim (0.3 - 3) \cdot 10^{34}$ y [55] has been predicted resulting in an 'upper bound' value for the proton lifetime. Also previous studies on SUSY theory have found the same decay channel $p \to K^+\overline{\nu}$ to be the dominant one with a lifetime range of $\tau \sim (10^{30} - 10^{35}$ y) [56].

The kaon produced in the dominant SUSY proton decay channel is 'invisible' in water Cherenkov detectors because its momentum is below the threshold for producing Cherenkov light ($T_{th}(\mathrm{K}^+) = 253$ MeV). For this reason, the Super-Kamiokande experiment could only perform an indirect measurement with efficiencies of 4.4% and 6.5% corresponding to two different meth-

ods [57]. The lower limit that they reach at 90% C.L. is $\tau = 2.3 \cdot 10^{33}$ y [58], which is about a factor of two worse than the limit given above for the channel $p \to e^+\pi^0$.

3.3 Supergravity

In supergravity models, proton decay proceeds mainly through the exchange of superheavy Higgsino and Higgs color-triplet particles. In those models, the gauge hierarchy requires for the Higgs mass $M_H < M_{GUT}$ and places the unification mass into the range $0.4 \cdot 10^{16} < M_{GUT} < 1.6 \cdot 10^{16}$ GeV [59].

Those theories provide also predictions for the possible decay channels of the proton. The dominant mode here is $p \to \pi^+\overline{\nu}$ with a branching ratio of 65.7%. However, again the proton decay mode $p \to K^+\overline{\nu}$ is predicted with a branching ratio of 33.5% [60].

Lifetime of Proton in LENA

To test the validity of these theories, a limit of some times 10^{34} or even 10^{35} has to be achieved for the decay channel $p \to K^+\overline{\nu}$. The LENA experiment can be expected to reach this goal or at least be quite close to it. As it will be presented in Chapter Results, from the simulation performed a limit of $\tau > 4 \cdot 10^{34}$ for the lifetime can be achieved.

Chapter 4

Detection Mechanism

The protons expected to decay in the LENA detector are the ones from the molecules of the liquid scintillator itself. That means that LENA is, for the proton decay, target and detector at the same time. Within the detector volume, about $1.45 \cdot 10^{34}$ protons, both from H- and C-nuclei , are candidates for the decay. This number has been calculated taking into account the chemical composition of PXE, $C_{16}H_{18}$ (see Chapter The LENA Experiment), its density (0.985 g/cm^3) and its molecular weight (210.3 a.m.u.). Protons from H nulei are called free protons. It is assumed that proton decay should occur in equal probability for both free and bound ones.

The decay products of the proton will produce, due to ionization processes in the PXE molecules, scintillation light with a mean wavelength of approximately 430 nm. This light will propagate through the detector to the walls where photomultipliers are placed to collect it.

In this chapter, an analysis of the event structure of proton decay from H- and C-nuclei is described and also the microscopic details of the decay mechanism are given.

4.1 Free Proton Decay

In the case of protons from H-nuclei ($0.23 \cdot 10^{34}$ protons in the fiducial volume of LENA), the decay problem is simplified because those protons decay at rest. Therefore, the proton decaying in the channel $p \rightarrow K^+ \overline{\nu}$ can be considered a two-body decay problem where K^+ and $\overline{\nu}$ always receive the same energy. The energy corresponding to the mass of the proton, $m_p = 938.3$ MeV is thereby given to the decay products. Using relativistic kinematics, it can be easily calculated that the particles receive fixed kinetic energies, the neu-

trino 339 MeV and the kaon 105 MeV.

In LENA, the kaon will cause a prompt mono-energetic signal while the neutrino escapes without producing any detectable signal. After $\tau(K^+) = 12.8$ ns, the kaon decays via $K^+ \to \mu^+\nu_\mu$ with a probability of 63.43 %. The kaon decays 90% of the times at rest [57] and from this kaon decay, a second mono-energetic signal arises, corresponding to the μ^+ with 152 MeV kinetic energy. Later, after $\tau(\mu^+) = 2.2$ μs, also the muon will decay: $\mu^+ \to e^+\nu_e\overline{\nu}_\mu$, the e^+ will produce a third long-delay signal. Since the last decay is a three body decay, the e^+ does not have a fix energy but a spectrum.

With a smaller probability, 21.13 %, the kaon decays, alternatively, via $K^+ \to \pi^+\pi^0$. The π^+ deposits its kinetic energy (108 MeV) in the detector. The π^0 decays almost immediately, within $\tau(\pi^0) = 8.4 \cdot 10^{-8}$ ns, into two gammas with a total energy being equal to the sum of the kinetic energy of the π^0 (111 MeV) and its rest mass ($m_{\pi^0} = 135$ MeV). These gammas can be seen in the detector as electromagnetic showers. Thus again there are two mono-energetic signals, firstly the kaon and secondly the one corresponding to the sum of the kinetic energy of the π^+ and the energy of the gammas. Again, there will be a third long-delayed signal from the succeeding decay ($\pi^+ \to \mu^+\nu_\mu$ and $\mu^+ \to e^+\nu_e\overline{\nu}_\mu$). Only these two most likely decay channels are considered in the analysis.

4.2 Proton Decay in C-Nuclei

Since the protons of the C-nuclei ($1.22 \cdot 10^{34}$ protons) belong to the nucleus, one has to consider further nuclear effects on the proton decay. In this section the binding energy of the proton in the nucleus and the Fermi-motion are discussed. At the end, the processing of these effects is explained in order to explain the input data used in the simulation performed (see Chapter Simulation).

4.2.1 Binding Energy

Since the protons are bound to the nucleus their effective mass will be reduced by the binding energy. The proton energy available for distribution between the decay products, will be $M_p' = M_p - E_b$, where M_p' is the modified proton mass, $M_p = 938.3$ MeV is the rest mass of the proton and E_b is the nuclear binding energy. The value of the binding energy E_b comes from gaussian probability functions which are centered at 37 MeV and 16 MeV

for protons in s-state and p-states respectively for C-nuclei [61].

In our case, taking into account the shell model for nuclei, from the six protons of ^{12}C, two of them will be in an s-state and the other four in p-states. In figure 4.1 data points of proton separation energy spectra for ^{12}C of a scattering experiment ^{12}C(e, e'p) [61] is given. For different recoil momentum intervals are also represented: solid curves, result of a fit with the momentum distributions calculated by Elton and Swift [62] and dashed curves showing the contribution from the 1p and 1s states.

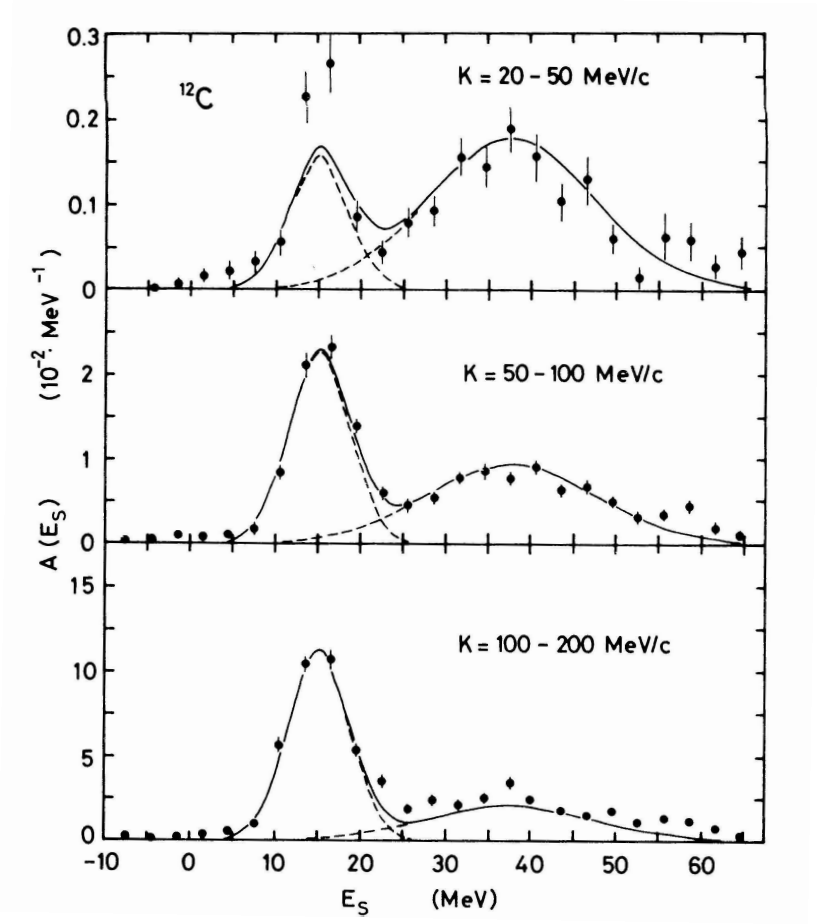

Figure 4.1: Data points of proton separation energy spectra for ^{12}C. The solid curves are the result of a fit with the momentum distributions calculated by Elton and Swift [62]. The dashed curves show the contribution from the 1p and 1s states [61].

4.2.2 Fermi Motion

In case of a proton decay in a nucleus, e.g., carbon, decay kinematics are different from the free proton due to the Fermi motion of the proton. This Fermi momenta have been measured by electron scattering on ^{12}C [61]. The distribution of the Fermi momenta for s-state and p-state are shown in figure 4.2 as derived from the measurment [61]. From the figure it can be seen that the maximum momentum is about 250 MeV/c.

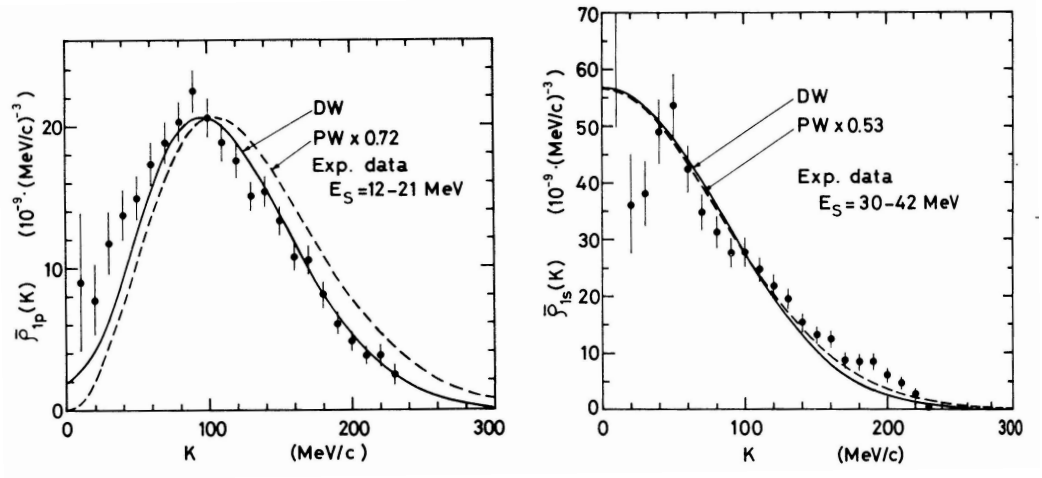

Figure 4.2: Distribution of the Fermi momenta measured in an electron scattering experiment [61] for protons in $1s_{1/2}$- (right figure) and $1p_{3/2}$-state (left figure) in ^{12}C. Data point are arbitrarily normalized. The lines represent the calculated momentum distributions using the bound-state potential given in [62].

Binding Energy and Fermi Motion Effects in the Proton Decay

In order to quantitatively estimate the kinetic energy change of the decay particles of the proton, various decay processes have been calculated. First of all, the mass of the proton was modified due to the binding energy giving to it the values already mentioned above. Then, two extreme cases were considered: the neutrino, moving after the decay, in the direction of the original proton and the neutrino moving in the opposite direction. The momentum of the proton was chosen to be maximal, corresponding to a Fermi momentum $\sim$250 MeV/c.

To calculate the relativistic kinematics of the decay including the two effects described, two equations for the conservation of energy and momentum were written[1].

$$E_p = E_{K^+} + E_{\overline{\nu}} \tag{4.1}$$

$$\sqrt{{m_p}^2 + {p_p}^2} = \sqrt{{m_{K^+}}^2 + {p_{K^+}}^2} + p_{\overline{\nu}}$$

$$p_p = p_{K^+} + p_{\overline{\nu}} \tag{4.2}$$

where $m_p = 938.3$ MeV, $m_{K^+} = 493.7$ MeV and $p_p = 250$ MeV/c. For this problem, the neutrino mass has been considered negligible, $m_\nu \sim 0$. In the momentum conservation equation, no vectors are represented because the limit cases occur in x axis.

By solving the ecuations 4.1 and 4.2, the limiting values of the kinetic energy of the kaon are: (25.1−198.8) MeV for the s-state and (30.0−207.2) MeV for the p-state. These limiting values correspond to the two cases where the neutrino moves in the direction of the proton and where the kaon moves in the proton direction.

As a first approximation to a realistic simulation (see Chapter Simulation) all kaons were generated with 105 MeV. Only later, in the analysis of the simulation data, the energy ranges given for the kinetic energy of the kaon have been taken into account. Therefore, the energy windows taken in the analysis are wide enough to include for the kaon the effects discused bove. Further simulations are planned to be performanced, where an initial energy spectrum of the kaon including both effects is used.

[1] $E^2 = {m_0}^2 c^4 + p^2 c^2$ with $c = 1$.

Chapter 5

Background

In this chapter the sources of background events that affect the energy region of the proton decay in the channel $p \to K^+\overline{\nu}$ is presented. For the atmospheric neutrinos which are the most important background, the rate measured by the Superkamiokande experiment is used.

5.1 Atmospheric Neutrinos ν_μ

The main background source in the energy range of the proton decay are muon neutrinos ν_μ produced by cosmic ray interactions in the atmosphere. Atmospheric ν_μ can interact with the scintillator producing muons in the energy range where the search for the proton decay is performed. The rate of these events in the relevant energy range can be derived from the Superkamiokande measurements [58]. Figure 5.1 shows data points of the number of muon events produced by atmospheric neutrinos in the Superkamiokande experiment. Also a Monte Carlo simulation of the atmospheric neutrinos and of the proton decay is presented.

From this data we find an event rate for Superkamiokande of:

$$\Gamma \sim 4.8 \cdot 10^{-2} (\mathrm{MeV}^{-1}\mathrm{kt}^{-1}\mathrm{y}^{-1}) \tag{5.1}$$

where the energy window and the amount of liquid scintillator have to be introduced in MeV and kt, respectively. In order to calculate this rate, first the number of events within their energy window was taken ($\sim$ 181 events) and then this value was devided by the mass of the Superkamiokande fiducial volume (22.5 kt), the energy window (41 MeV) and the measuring time (1489 days).

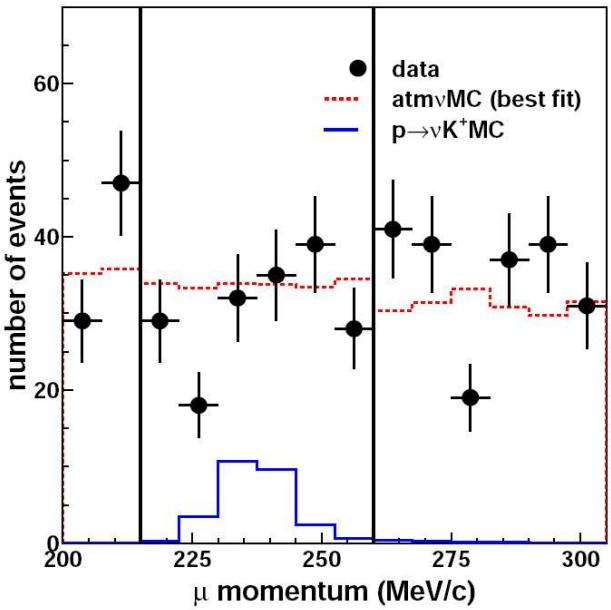

Figure 5.1: Muon rate in Superkamiokande as a function of the muon momentum. The solid points are experimental data. The two lines represent Monte Carlo simulations of atmospheric neutrinos that create muons in the detector and of the proton decay in the channel $p \to K^+\overline{\nu}$ [58].

Introducing the LENA fiducial volume (45 kt) and the energy window that will be taken (550 MeV, see Chapter Analysis) a backgroung rate of $\Gamma \sim 1190.4\ \mathrm{y}^{-1}$ results. A pulse shape analysis is required to discriminate between these background signals and proton decay candidates.

5.2 Fast Neutrons

Very fast neutrons, generated by spallation processes of cosmic muons outside the detector, may reach the scintillator causing background events. These neutrons are slowed down through scattering processes and the recoil protons may produce a background signal in the detector. However, only neutrons produced by muons passing close to the detector but not through the veto, have to be taken into account. In addition, these signals can be tagged as the neutrons are captured by hydrogen in the scintillator after $\sim 200\ \mu$s, producing an observable 2.2 MeV gamma.

Chapter 6

Simulation

In order to quantitatively estimate the potential of the LENA detector to measure the proton lifetime, a Monte Carlo simulation of the proton decay in the channel $p \rightarrow K^{+}\overline{\nu}$ has been performed. This chapter describes this simulation, covering both the detector implementation and the obtained signal output. Concerning the detector description the focus is on the optical processes that take place in the liquid scintillator. The section on the simulation output shows the signal structure of proton decay and background events (compare with chapters 4 and 5).

6.1 Geant4

Geant4 is a C++ commonly used toolkit that simulates the passage of particles through matter [63]. This software was developed at CERN in order to give a complete set of tools for all domains of detector simulation. It was originally designed for high energy physics simulations but due to its abundant set of physical processes it can handle the diverse interactions of particles with matter across a wide energy range. Thus Geant4 has now a multi-disciplinary nature.

As Geant4 is based on the Standard Model of Particle Physics, the protons of the simulated liquid scintillator do not decay by themselves. To perform the simulation the event generator was programmed to produce K^{+} particles of 105 MeV kinetic energy in different positions of the detector volume and with random directions of motion. The volume considered was a cylinder of 12 m radius, which has been called (see Detector Design) fiducial volume. In order to investigate the dependence of the light output on the event position, the kaons were generated in different radial positions (center, 3, 6, 9 and 11.5 m) of the detector.

In figure 6.1, the visualization output of one proton decay event at the top of the detector is plotted. First, there is a box that is the defined volume of the experimental hall and then a cylinder that represents the detector volume. Perpendicular to the hall walls, there are three straight lines in red, blue and green that are the x, y and z axes. In Geant4 the particles are represented with different colours depending on their charge, green for neutral, blue for positively and red for negatively charged particles, respectively. In the figure only green lines can be seen, most them (all inside the cylinder) represent light rays whereas straight lines that leave the detector depict neutrinos. It can be seen that the light scatters and that sometimes it is absorbed before reaching the walls. The tracks corresponding to the K^+ and its charged decay products can not be seen because of being covered by the light tracks.

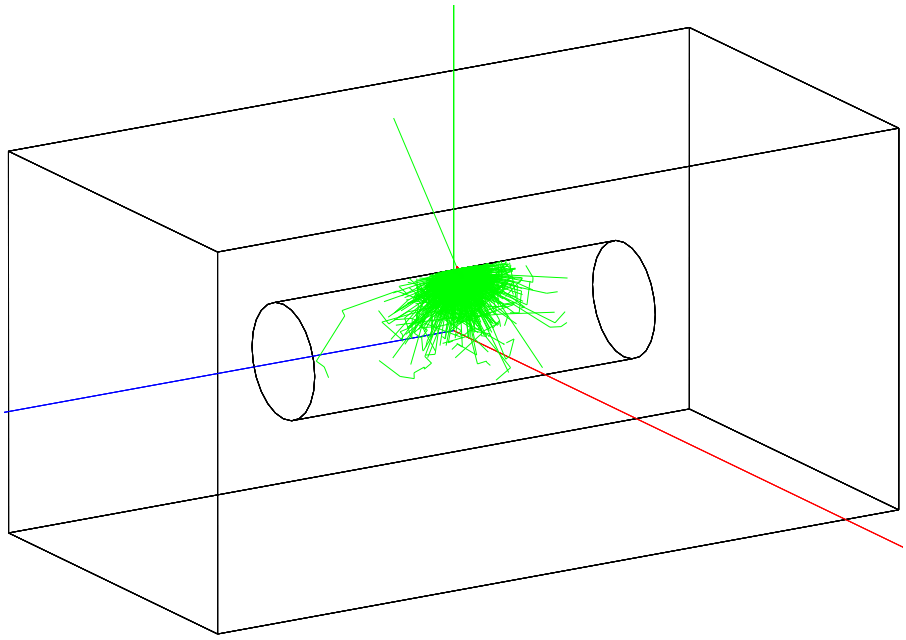

Figure 6.1: Output visualisation from LENA simulation. The green lines represent neutral particles, the straight ones that go through the detector depict neutrinos and the ones that scatter and are absorbed are light rays produced in the scintillator.

6.2 Detector Implementation

6.2.1 Physics Processes

Physics processes describe how particles interact with a material. Some major categories of processes are provided by Geant4: electromagnetic, hadronic, transportation, decay and optical. From these Geant4 physics lists special attention was paid to the optical processes as scintillation, Cherenkov light production, Rayleigh scattering and light absorption. For the last two processes a scattering and absorption length of $\lambda_s = 60$ m and $\lambda_a = 12$ m, respectively were assumed. With these numbers an effective attenuation length of $\lambda = 10$ m results:

$$\lambda = \frac{\lambda_s \cdot \lambda_a}{\lambda_s + \lambda_a} \tag{6.1}$$

This is a quite conservative approach compared to the measured value of $\lambda = 12$ m [38]. However, even with this smaller value a light yield of ~ 110 pe/MeV was obtained. Within this simulation, it was also possible to verify that the kaons decay according to the branching ratios for the different channels stated in [40].

6.2.2 Quenching Effects

The amount of light emitted by a scintillating material is not strictly proportional to the energy deposited by the ionizing particle. In reality, it is a complex function of the energy, the type of particle and the specific ionization [64]. Geant4 uses a light yield depending only on the energy of the particle. To take into account the so called quenching effects, the semi-empirical Birk's formula [65] has been introduced into the code:

$$\frac{\mathrm{d}L}{\mathrm{d}x} = \frac{A\frac{\mathrm{d}E}{\mathrm{d}x}}{1 + kB\frac{\mathrm{d}E}{\mathrm{d}x}} \tag{6.2}$$

According to equation 6.2, the programm calculates in every step the deposited energy ($\mathrm{d}E$) within the distance ($\mathrm{d}x$) travelled by the particle and derives the light output ($\mathrm{d}L/\mathrm{d}x$).

The parameters of this formula are A: absolute scintillation efficiency and kB: parameter relating the density of ionization centers to $\frac{\mathrm{d}E}{\mathrm{d}x}$. Both are specific values for every scintillator and are obtained from experimental data. For the simulation, $A = 10^3$ photons/MeV and $kB = 1.5 \cdot 10^{-3}$ cm/MeV have been taken from studies performed by the Borexino Collaboration [66]. Basically, the parameter A is the light output for electrons. By taking this light output measured for electrons (A) and the corresponding light output for alpha particles ($\mathrm{d}L/\mathrm{d}x$) and substituting both into equation 6.2, the value of kB is obtained.

6.2.3 Photomultipliers

Also the photomultipliers have been introduced in the simulation but not as physical objects. Only their effects concerning the output signal were taken into account. They were assumed to have an efficiency of 17 % and a time jitter of $\sigma = 1$ ns originating from the transit time of electrons through the photomultipliers and from the statistical noise. These features are known because the type of photomultiplier expected to be used in LENA, has already been tested in other experiments [67].

6.3 Simulation Output

In this section, the output results of the simulation are presented. First, the energy deposited by charged particles due to inelastic collisions in the scintillator and second, the number of photoelectrons produced by the light once it has hit the photomultipliers. Both, the deposited energy and the number of photoelectrons are given as a function of the real time, that is measured by Geant4.

6.3.1 Energy Deposited in the Scintillator

Figure 6.2 presents the energy deposited in the scintillator in timesteps of 0.1 ns as calculated by Geant4. At time 0 ns, the kaon is produced and deposits its energy during 1.2 ns. Looking at the figure, it can be seen that the sum of the energy deposited by the kaon is 105 MeV, the kinetic energy with which it is produced. In this case, the kaon decays into a muon and a neutrino after $\sim$ 6 ns. The muon deposits its kinetic energy of 152 MeV during about 2 ns and later (outside the picture) decays into a positron and two neutrinos.

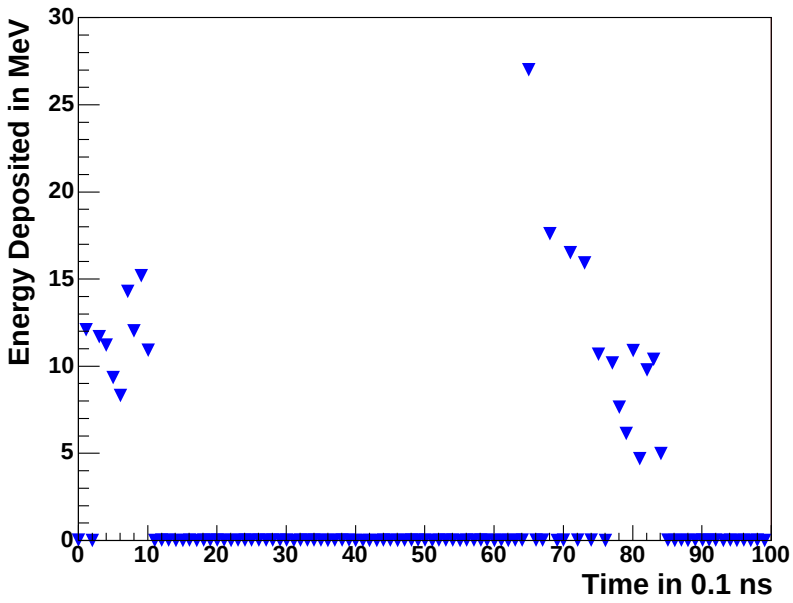

Figure 6.2: Energy deposited by a kaon and a muon as fuction of time. The first points correspond to the kaon which deposits its energy within 1.2 ns. In the case shown, after about 6 ns the kaon decays into a muon and a neutrino, the energy deposition of the muon can be seen between 6.5 and 8.5 ns.

6.3.2 Signal Structure

Figure 6.3 depicts signals in LENA, the number of photoelectrons detected in the photomultipliers as a function of time in ns. As the kaon decays within a relatively short time ($\tau(\mathrm{K}^+) = 12.8$ ns), the signature of such an event will consist of two shortly delayed signals (see Chapter Detection Mechanism). Examples of proton decay signals where the separation is clearly visible (top), where it is almost hidden in the risetime (middle) and of a muon background signal (botton) can be seen in figure. The on-set time of these examples is 60 ns as the events are generated at the center of the detector and the photons need this time to reach the photomultipliers on the walls.

The better the two signals can be separated, the better the background suppression will be. In the cases where the kaon decays at relatively late times $t > 10$ ns, the two peaks can be easily separated; in all other cases, only a shoulder within the risetime can be seen. In order to distinguish the real proton decay signals from muon background events, a pulse shape analysis that will be described in the next chapter, is required.

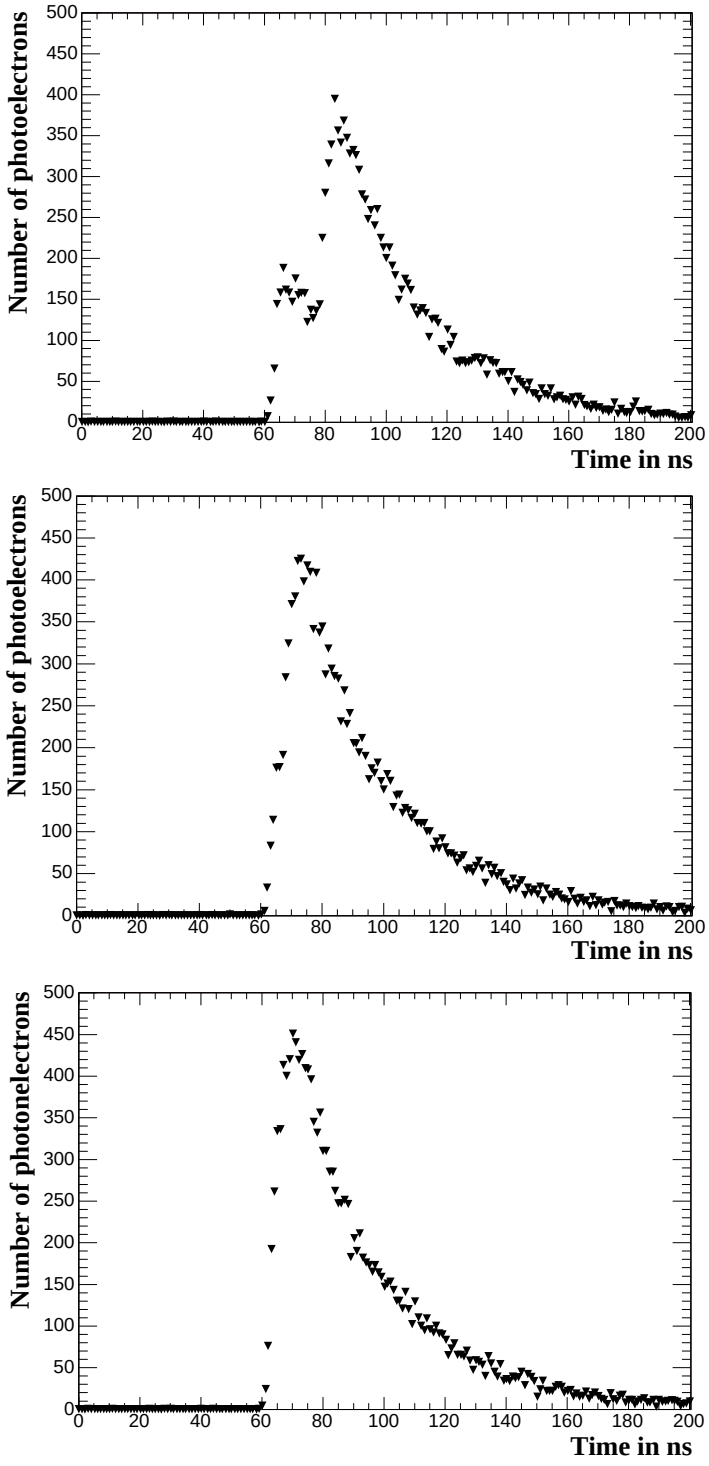

Figure 6.3: Proton decay signals where the kaon decays after 18 ns (top) and after 5 ns (middle). The bottom panel shows a ν_μ background signal. For further details see explanation in the text.

Chapter 7

Analysis

This chapter explains the tools used to store, read and analyse the output data from the Geant4 simulation performed. On this basis, the general analysis procedure used for the results of this thesis is described. Finally, a summary of the simulation runs is given.

7.1 ROOT

7.1.1 The Output ROOT Tree

ROOT is an object oriented analysis framework that was developed at CERN. It provides classes which support the efficient processing of event based data trees. Basically, the tree contains information about the events, which constitute the top level and the parameters of each track of an event. In the simulations performed, the output data was storaged in such a tree. The parameters taken were the number of photoelectrons received after the photomultipliers and the corresponding time vector.

7.1.2 The Analysis Program

For the analysis of the ROOT trees a C++ program is used. The basic idea is the following: loop over all events of the tree and over all tracks, select the risetime of the signals and discriminate between the proton decay signal and the background events. The cuts applied to the data will be explained in detail in the coming subsections.

Pulse Shape Analysis: Time Cut

A first step towards a pulse shape analysis has been taken in order to quantify the signal and background discrimination. For these simulations, the particles were generated and the light produced was followed through the scintillator including scattering and absorption as well as the photomultiplier efficiency and its time jitter. This results in the number of photoelectrons detected as a function of time (see Chapter Simulation). In order to analyze the risetime of the resulting signal, the maximum number of photoelectrons is taken and the 15 % and the 85 % values of the maximum signal height are determined. The difference of the two corresponding time values is plotted in figure 7.1 for 10 000 proton decays and 20 000 background events.

As an example, the effect of a cut at 7 ns is shown in this figure. The analysis performed for 20 000 background events shows that applying such a cut, a background reduction by a factor of $\sim 2 \cdot 10^4$ is achieved. The background plot shown applies only to the channel $p \to K^+\overline{\nu}$ and $K^+ \to \pi^+\pi^0$. A similar simulation has been performed for the channel $p \to K^+\overline{\nu}$ and $K^+ \to \mu^+\nu_\mu$, resulting in an equivalent result where the same rejection factor is obtained. An efficiency of $\varepsilon_T = 0.65$ results after this time cut as only 35% of the signals are lost.

As the analysis is performed within the signal risetime, the latter part of the signal is lost. Further pulse shape analysis where the complete signal is taken can be applied. Possible ideas are: Fourier analysis, fitting curves and neuronal network.

Energy Cut

In order to further improve the signal to background separation a cut in the energy spectrum can be applied. In figure 7.2, the distribution of the number of photoelectrons coming from free proton decay events at the center of the detector as seen in the photomultipliers is plotted.

Two peaks can clearly be identified, corresponding to the two main decay channels of the kaon. They are related to the energies of 257 and 459 MeV respectively, which is the sum of the energies deposited by the kaon and its decay products. To take into account also the protons from C-nuclei (see section Detection Mechanism), an energy window of 300 MeV for each channel has been set. The two energy windows overlap resulting in a final window of 550 MeV. An efficiency of $\varepsilon_E = 0.995$ results, that means that only five out of 1000 possible proton decay events are not inside our energy cut.

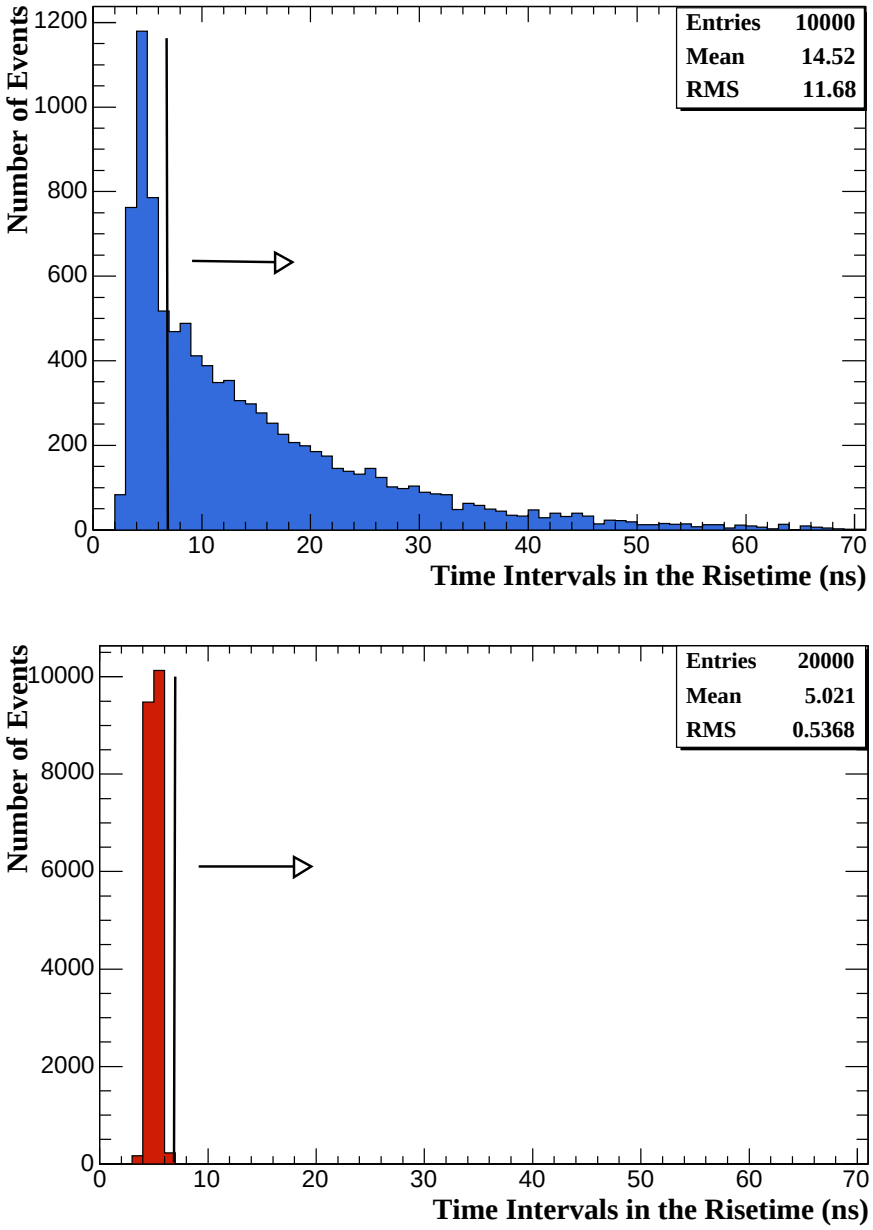

Figure 7.1: Distribution of time intervals in the risetimes for 10 000 proton decay (top) and 20 000 muon background signals (bottom). A cut at 7 ns yields a reduction factor of $\sim 2 \cdot 10^4$ on background events whereas the efficiency for observing a proton decay $p \to K^+\overline{\nu}$ is 65%.

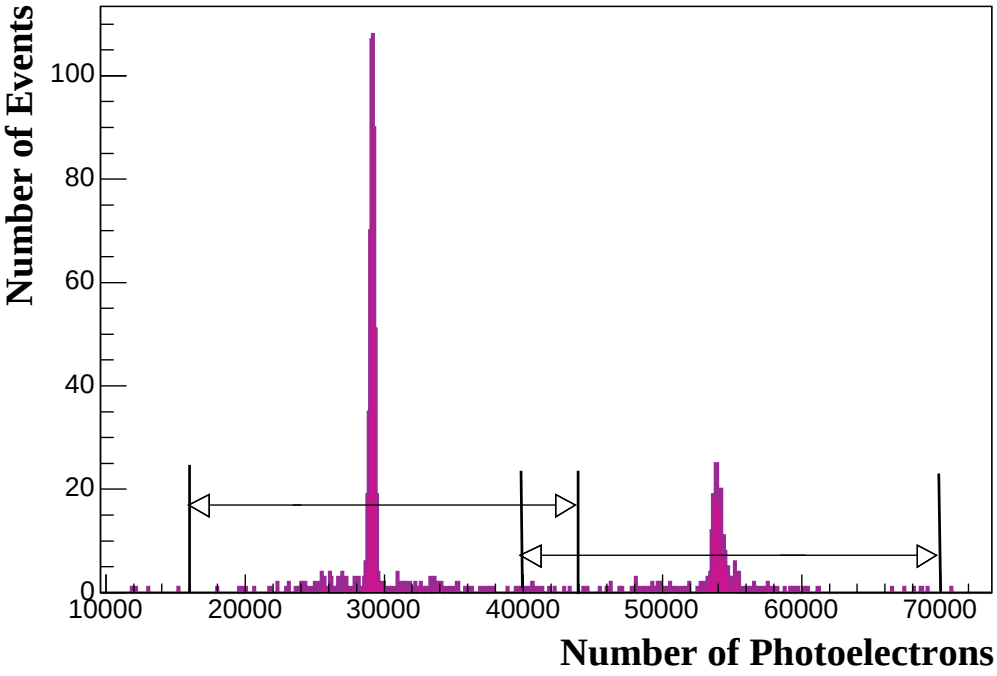

Figure 7.2: Distribution of the number of photoelectrons produced in the photomultipliers coming from proton decay events at the center of the detector. The cuts performed for the two main channels for the kaon decay (at 257 and 459 MeV) are shown. It can be appreciated that the energy windows taken overlap resulting in a total window of 5500 Photoelectrons $\simeq$ 550 MeV.

The signals outside the two main peaks correspond mainly to kaon decay channels not considered in the analysis. There is also a small loss due to inelastic hadronic interactions of the decay particles before they are stopped.

7.2 Summary of the Simulations Performed

Two kinds of input data were used for the Monte Carlo simulations, first proton decay events: kaons of 105 MeV as primary particles, and second background: muon with energies corresponding to the signals of proton decay expected. The muons were produced with energies of 257 and 459 MeV respectively because this is the sum of the energy of the kaon and the kaon decay products that make a signal in the detector. The first energy correspond to the channels $p \rightarrow K^+\overline{\nu}$ and $K^+ \rightarrow \mu^+\nu_\mu$, the sum of the kaon and the muon energy, and the second to the channels $p \rightarrow K^+\overline{\nu}$ and $K^+ \rightarrow \pi^+\pi^0$, the sum of the kaon and the two pions energies. Both, proton decay and

Radial Position	Proton Decay	257 MeV Muon	459 MeV Muon
Center	20 000	20 000	20 000
Center	1 000	1 000	1 000
3.0 m	1 000	1 000	1 000
6.0 m	1 000	1 000	1 000
9.0 m	1 000	1 000	1 000
11.5 m	1 000	1 000	1 000

Table 7.1: Number of events simulated, proton decay and muon background signals of 257 and 459 MeV in different radial positions in the detector.

background events were produced in different radial positions in the detector in order to check the effect of the position on the light output. The dependence on the event position will be discussed in the next chapter. In table 7.1 the number of events simulated is summarized. To look further into the background suppression 20 000 events were simulated at the center of the detector. For each of the other positions 1 000 events were simulated.

Chapter 8

Results

In this chapter, the two most important parts of the results are presented, the detector efficiency as determined from the simulation and the lifetime limits reachable with LENA.

8.1 Detector Efficiency

Once the time cut and the energy cut have been applied, the final efficiency of the proton decay detection in the considered channels, $\varepsilon = \varepsilon_E \cdot \varepsilon_T$ can be calculated. In table 8.1 the efficiencies for events at different radial positions in the detector are presented as well as the background rates for the same positions. No dependence of the efficiency on the event position within the statistical error has been found as it can be appreciated in the table 8.1.

The background rates presented have been obtained by multiplying the background rate in LENA detector derived from the Superkamiokande exper-

Radial Position	ε_T	ε_E	ε	B (y^{-1})
Center	0.649	0.995	0.65±0.04	0.05
3.0 m	0.675	0.994	0.67±0.04	0.05
6.0 m	0.650	0.994	0.65±0.04	0.05
9.0 m	0.679	0.995	0.68±0.04	0.05
11.5 m	0.666	0.995	0.66±0.04	0.05

Table 8.1: For 1000 events produced in different radial positions in the detector, the efficiency in the time-cut ε_T, the efficiency in the energy-cut ε_E and the background rate B are given.

iment (1190.4 y^{-1}, see chapter Background) and the background suppression from the time cut ($2 \cdot 10^{-4}$, see Chapter Analysis). As the detector is symmetrical along the cylinder axis the points considered are at the middle of the z axis and at different radial distances. For example, for the 20 000 decays taking place at the center of the detector an efficiency of 65% has been obtained.

8.2 Proton Decay Sensitivity

The proton fulfils the radioactive decay law and thus the activity for its decay is given by:

$$a = \epsilon N_p t_m / \tau \tag{8.1}$$

where ε is the total efficiency already explained in the previous section; $N_p = 1.45 \cdot 10^{34}$ is the number of protons in the fiducial volume; t_m is the measuring time and τ is the lifetime of the proton.

For the current proton lifetime limit ($\tau = 2.3 \cdot 10^{33}$ y) [54], about 40.7 proton decay events would be observed in LENA after ten years of measuring time with an upper limit of about 0.5 background events. If no signal is seen in the detector, the lower limit for the lifetime of the proton can be determined. To calculate the lower limit for the proton lifetime the Poisson distribution was used. The Poisson distribution occurs when the probability p$\rightarrow$ 0 and the number of trials N$\rightarrow \infty$, such that the mean a = N.p remains finite. The probability of observing r events is given by:

$$P(r) = \frac{a^r e^{-a}}{r!} \tag{8.2}$$

If no events are measured after ten years measuring time, $r = 0$ and $P(0) = e^{-a}$, the activity at 90% confidence level can be easily calculated. The corresponding lifetime of the proton reachable will be placed at $\tau > 4 \cdot 10^{34}$ y at 90% (C.L).

The succes in reaching this limit is based on the distinct pulse shape of the proton decay mode $p \rightarrow K^+ \overline{\nu}$ which is clearly observable in the LENA

detector. Basically, no energy cut was used and hence the efficiency for observing the proton decay including free and bound protons is high. This is the substancial difference to the Superkamiokande experiment, where the total efficiency for this decay mode is of 4.4% and 6.5% for two different methods [57]. Since the value predicted by the theory for the proton decay in this channel is in the order of magnitud of the value resulting from our simulation, it is obvious that LENA measurements would have a deep impact on the research field of proton decay.

Chapter 9

Conclusions and Outlook

LENA is a large-volume liquid-scintillator detector proposed to cover a rich physics program including particle, astroparticle and geophysics. It is foreseen to use PXE as scintillating material and photomultipliers for signal readout. In the current design a mass of ~ 50 kt and ~ 12000 photomultiplier will be required which would be much smaller than a comparable water Cherenkov detector, e.g., the proposed Hyperkamiokande experiment with 1 Mt of water and $100000 - 200000$ photomultipliers [53].

One major point of interest will be the search for proton decay events because of the important implications for particle physics. In this thesis a detailed simulation has been performed for the decay channel $p \rightarrow K^+\overline{\nu}$. For the detector implementation, special attention has been paid to the optical processes taking place in the scintillator, the quenching effects and the properties of the photomultipliers.

From this simulation an efficiency of $\varepsilon = 65\%$ has been obtained for the detection of the proton decay in the LENA detector. The underlying analysis is based on a pulse shape analysis and an energy cut for background substraction. No strong dependence on the radial event position has been found. Taking into account the current limit for the proton lifetime for this channel ($\tau > 2.3 \cdot 10^{33}$ y [58]), 40.7 proton decay events and an upper limit of 1 background event are expected to be observed in LENA after 10 years of measuring time. If no event is detected a lower limit of $\tau > 4 \cdot 10^{34}$ y could be reached. It should be pointed out that the also proposed future experiment Hyperkamiokande will not be able to surpass this value [53].

Several ideas exist to further improve the pulse shape analysis and therefore the efficiency for the proton decay for the channel mentioned above, for

example a Fourier analysis of the signal pulses could be applied. This analysis could further improve the signal to background separation. Although other probably subdominant proton decay channels as well as other possible background sources, e.g., K^+ production via high energy atmospheric neutrinos [53] have to be studied, we can conclude already now that the LENA detector will have a great potential concerning the search for proton decay events.

For future research and feasibility studies a deeper knowledge of the scintillator material PXE and its optical properties is needed, for example the precise measurement of the absorption and scattering lengths separately [68]. This, in combination with the simulation will allow a full description and understanding of the LENA detector. The simulation itself constitutes a flexible tool to look also into other physical processes of interest, for example the search for supernovae neutrinos.

Bibliography

[1] R. Davis, Prog. Part. Nucl. Phys. 32 (1994) 13.

[2] K. Hirata et al., Phys. Rev. Lett. 58 (1987) 1490.

[3] R. M. Bionta et al., Phys. Rev. Lett. 58 (1987) 1494.

[4] C. B. Bratton et al., Phys. Rev. D 37 (1988) 3361.

[5] K. Hirata et al., Phys. Rev. D 38 (1988) 448.

[6] The SNO Collaboration, http://www.sno.phy.queensu.ca

[7] The GALLEX Collaboration, W. Hampel et al., Phys. Lett. B 447 (1999) 127.

[8] The SAGE Collaboration, J. N. Abdurashitov et al., Phys. Rev. Lett. 83 (1999) 4686.

[9] The GNO Collaboration, M. Altmann et al., hep-ex/0504037 (2005).

[10] The SNO Collaboration, Q. R. Ahmad et al., Phys. Rev. Lett. 89 (2002) 011301.

[11] The KamLAND Collaboration, K. Eguchi et al., Phys. Rev. Lett. 90 (2003) 021802.

[12] The Superkamiokande Collaboration, S. Fukuda et al., Phys. Lett. B 539 (2002) 179.

[13] The IMB Collaboration, R. Clark et al., Phys. Rev. Lett. 79 (1997) 345.

[14] E. D. Church et al., Phys. Rev. D 66 (2002) 013001.

[15] The MinibooNE Collaboration, H. Ray et al., "Meeting of the Division of Particles and Fields, DPF2004", hep-ex/0411022 (2004).

[16] N. Schmitz, "Neutrinophysik", Teubner-Studienbücher: Physik, Stuttgart (1997).

[17] Yu. F. Pirogov, Phys. Atom. Nucl. 65 (2002) 109, hep-ph/0005290.

[18] C. Weinheimer, Nucl. Phys. B (Proc. Suppl.) 118 (2003) 279.

[19] V. M. Lobashev et al., Nucl. Phys. B (Proc. Suppl.) 118 (2003) 282.

[20] V. Barger, D. Marfatia and A. Tregre, Phys. Lett. B 595 (2004) 55.

[21] The BOREXINO Collaboration, Nucl. Instr. Meth. A 461 (2001) 327.

[22] The Superkamiokande Collaboration, M. Malek et al., Phys. Rev. Lett. 90 (2003) 061101.

[23] S. Ando, K. Sato and T. Totani, Astropart. Phys. 18 (2003) 307.

[24] R. Tomas et al., astro-ph/0407132 (2004).

[25] H. T. Janka et al., astro-ph/0212314 (2002).

[26] H. T. Janka et al., astro-ph/0212316 (2002).

[27] A. S. Dighe et al., JCAP 0401 (2004) 004.

[28] A. S. Dighe et al., JCAP 0306 (2003) 006.

[29] T. Hagner et al., Astropart. Phys. 14 (2000) 33.

[30] A. S. Dighe, Q. Y. Liu and A. Yu. Smirnov, hep-ph/9903329.

[31] S. P. Mikheyev and A. Yu Smirnov, Sov. J. Nucl. Phys. 42 (1985) 913.

[32] L. Wolfenstein, Phys. Rev. D 17 (1978) 2369.

[33] E. Kh. Akhmedov, S. T. Petcov and A. Yu Smirnov, Phys. Rev. D 48 (1993) 2167.

[34] G. Fiorentini, M. Lissia, F. Mantovani and R. Vannucci, hep-ph/0409152 (2004).

[35] K. Hochmuth, "The Angular Distribution of Geoneutrinos and their Detection with LENA", Diploma Thesis, Technical University of Munich, April 2005.

[36] M. Lindner, "XXth International Conference on Neutrino Physics and Astrophysics" May 25 - 30, Munich, Germany (2002), Springer Tracts Mod. Phys. 190 (2003) 209.

[37] L. Oberauer, F. von Feilitzsch and W. Potzel , Nucl. Phys. B (Proc. Suppl.) 138 (2005) 108.

[38] Stefan Schönert, submitted to NIM A, physics/0408032, (2004).

[39] C. Buck and M. Wurm, priv. communication.

[40] Particle Data Group, S. Eidelman et al., Phys. Lett. B 592 (2004) 1.

[41] S. L. Glashow, Nucl. Phys. 22 (1961) 579.

[42] S. Weinberg, Phys. Rev. Lett. 19 (1967) 1264.

[43] A. Salam, Proc. of the 8th Nobel Symposium on "Elementary particle theory, relativistic groups and analyticity", Stockholm, Sweden, 1968, edited by N. Svartholm (1969), 367.

[44] Ta-Pei Cheng and Ling-Fong Li, "Gauge theory of elementary particle physics", Clarendon Press, Oxford (1984).

[45] D. Bailin amd A. Love, "Introduction to Gauge Field Theory", Institute of Physics Publishing (1986), Revised in 1993.

[46] M. L. Cherry et al., Phys. Rev. Lett. 47 (1981) 1507.

[47] The Soudan 2 Collaboration, D. Wall et al., Phys. Rev. D 62 (2000) 092003.

[48] O. Saavedra et al., 1984. In "Nordkirchen 1984, Proceedings, Neutrino Physics and Astrophysics", 350.

[49] The Frejus Collaboration, C. Berger et al., Phys. Lett. B 269 (1991) 227.

[50] E. Aprile-Giboni et al., "AIP Conference Proceedings", May 1984 Volume 114, Issue 1, 77.

[51] The IMB Collaboration, R. Becker-Szendy et al., Phys. Rev. D 49 (1994) 2169.

[52] H. Georgi and S. L. Glashow, Phys. Rev. Lett. 32 (1974) 438.

[53] T. Hakaya, Nucl. Phys. B (Proc. Suppl.) 138 (2005) 376.

[54] E. T. Kearns, "Snowmass Conference", Snowmass Village, Colorado, 30 June-21 July (2001), http://hep.bu.edu/

[55] S. Raby, Proc. of "10th international conference on Supersymmetry and Unification of Fundamental Interactions SUSY'02", DESY, Hamburg, Germany, 17-23 June (2002), hep-ph/0211024 (2002).

[56] K. S. Babu, J. C. Pati and F. Wilczek, Phys. Lett. B 423 (1998) 337.

[57] The Superkamiokande Collaboration, Y. Hayato et al., Phys. Rev. Lett. 83 (1999) 1529.

[58] The Superkamiokande Collaboration, K. Kobayashi et al., hep-ex/0502026 (2005).

[59] P. Nath and R. Arnowit, Phys. Rev. D 38 (1988) 1479.

[60] R. Arnowit, A. H. Chamseddine and P. Nath, Phys. Lett. B 156 (1985) 215.

[61] K. Nakamura et al., Nucl. Phys. A 268 (1976) 381.

[62] L. R. B. Elton and A. Swift, Nucl. Phys. A 94 (1967) 52.

[63] The Geant4 Collaboration, S. Agostinelli et al., Nucl. Instr. Meth. A 506 (2003) 250.

[64] W.R. Leo, "Techniques for Nuclear and Particle Physics Experiments", Springer-Verlag, Berlin Heidelberg (1987).

[65] J. B. Birks, "The theory and Practice of Scintillation Counting", Pergamon Press, London (1964).

[66] H. O. Back et al., Phys. Lett. B 525 (2002) 29.

[67] G. Alimonti et al., Astropart. Phys. 16 (2002) 205.

[68] M. Wurm, priv. communication.

Acknowledgments

En primer lugar quiero agradecer mis padres la posibilidad que me han dado de poder estudiar la carrera de física. Sin su apoyo, sobretodo personal pero también económico no me hubiera sido posible acabar con éxito mis estudios ni poder realizar los programas de intercambio en Valencia y Múnich.

Ich danke Prof. von Feilitzsch für die Möglichkeit, in diese Gruppe rein gekommen zu sein, erst als Werkstudent and dann zu bleiben. Die nette Atmosphäre bei e15 finde ich sehr gut.

Vielen Dank mein Betreuer Prof. Lothar Oberauer der mir diese Diplomarbeit ermöglich hat. Von Ihm habe ich sehr viel Physik gelernt und er hat immer Zeit gefunden meine Fragen zu antworten. Duch die vielen Diskussionen hat er mich sehr für meine Arbeit motiviert, und ich hatte viel Spaß.

Walter Potzel will ich danken für die detaillierte und trotzdem schnelle Korrektur dieser Diplomarbeit. Für Theoriefragen war Prof. Lindner immer sehr hilfsbereit. Meine Bürokollegen, Ludwig Niedermeier, Davide D'Angelo und Christian Lendvai, haben mir geholfen, mich am Anfang zu Recht zu finden. Insbesondere Christian Grieb, der mir Geant4 beigebracht hat. Ohne die Hilfe von unserem Computer-Administrator Tobias Lachenmeier wäre ich nicht weit mit Linux gekommen. Und ohne die Hilfe von Beatrize van Bellen wäre ich bei der ganzen Papierbürokratie hilflos gewesen.

Danke meine Kollegen von LENA, Michael Wurm und Kathrin Hochmuth, für die immer gute Zusammenarbeit und dem 'Bayerische Background', den ich mitbekommen habe. Alle anderen, die ich leider nicht persönlich genannt habe, haben natürlich auch ihren Beitrag zu dieser tollen Atmosphäre.

Muchas gracias a Quirin Weitzel por su ayuda en innumerables ocasiones, por contestar mis preguntas sobre Geant4, ROOT o LaTeX, por discutir conmigo sobre física y por ayudarme con el idioma pero sobretodo por su apoyo en todo momento.